The Journal of Experimental Biology 202, 3011–3020 (1999)
Printed in Great Britain © The Company of Biologists Limited 1999
JEB2064

THE SUPRAMOLECULAR ORGANISATION OF FIBRILLIN-RICH MICROFIBRILS DETERMINES THE MECHANICAL PROPERTIES OF BOVINE ZONULAR FILAMENTS

D. M. WRIGHT[1,2], V. C. DUANCE[2], T. J. WESS[1,3], C. M. KIELTY[4] AND P. P. PURSLOW[1,*]

[1]*The Royal Veterinary and Agricultural University, 1958 Frederiksberg, Copenhagen, Denmark,* [2]*School of Biosciences, Cardiff University, Cardiff CF1 3US, UK,* [3]*Department of Biological and Molecular Sciences, University of Stirling, Stirling FK9 4LA, UK* and [4]*School of Biological Sciences, University of Manchester, Manchester M13 9PT, UK*

*Author for correspondence and present address: Kødområdet, MLI, KVL, Rolighedsvej 30, DK-1958 Frederiksberg C, Denmark (e-mail: ppp@kvl.dk)

Accepted 13 August; published on WWW 13 October 1999

Summary

The zonular filaments from the eyes of cows are rich in microfibrils containing fibrillin. Tensile tests, stress-relaxation tests and X-ray diffraction studies were used to study the relationship between the mechanical behaviour of zonular filaments and the molecular packing and structure of the fibrillin-rich microfibrils. Zonular filaments show a non-linear (J-shaped) stress–strain curve and appreciable stress-relaxation. It is proposed that the non-linear properties are due to local variations in waviness in the microfibrils or assemblies of microfibrils, which straighten out and become more regularly aligned with strain. Previous and current X-ray diffraction results consistently show a partial ordering of microfibrils in zonular filaments into staggered aggregates which become more ordered and laterally aligned on stretching. Although the removal and re-addition of Ca^{2+} is known to change the molecular structure of fibrillin, no effect was observed on the tensile properties of the zonular filaments. It is hypothesised that strain-induced deformation in the supramolecular aggregate packing may not be Ca^{2+}-sensitive but could dominate the mechanical behaviour of microfibrillar arrays in zonular filaments.

Key words: fibrillin, microfibril, elasticity, molecular structure, X-ray diffraction, mechanical properties.

Introduction

The ocular zonule is a network of fibres that suspends the lens from the ciliary body in the eye (Mayne et al., 1997). The forces involved in changing the shape of the lens to accommodate the eye are transmitted *via* the zonular network. Zonular filaments are rich in microfibrils, whose primary components are the structural glycoproteins fibrillin-1 and fibrillin-2. Fibrillin-rich microfibrils are widely distributed in extracellular matrices, such as skin, intramuscular connective tissue, blood vessels, ligaments and cartilage (Sakai et al., 1986; Kielty and Shuttleworth, 1995). In many extracellular matrices, microfibrils act as a template for elastin deposition, and so mature elastic fibres contain both elastin and fibrillin-rich microfibrils (Mecham and Heusar, 1991). However, the microfibrils of ocular zonules contain no detectable amounts of elastin (Waggett et al., 1993).

Microfibrils isolated from a wide variety of tissues appear in rotary-shadowed electron micrographs as beaded structures 10–14 nm wide with a bead+interbead axial unit repeat (*D*) of 33–165 nm, with the most common average *D* period of 56 nm (Keene et al., 1991; Sherratt et al, 1997; Wright et al., 1994). This 400 % variation in *D* period suggests that the microfibrils are highly extensible. McConnell et al. (1996) have demonstrated changes in the *D* periodicity in microfibrils within the aorta of lobsters when distended and fixed under pressure.

Fibrillin-1 and fibrillin-2 contain 47 epidermal growth-factor-like domains, 43 of which have a consensus sequence for Ca^{2+} binding (Sakai et al., 1991). Fibrillin is thought to contribute to both the bead and interbead regions of the microfibril, although there are other molecules present (Reinhardt et al., 1996; Gibson et al., 1996; Kielty et al., 1996; Taipale et al., 1996). The structure of the microfibril is greatly influenced by Ca^{2+}. Removal of Ca^{2+} disrupts molecular packing (Kielty and Shuttleworth, 1993), and recent studies suggest that removal of Ca^{2+} results in decreases in interbead periodicity and increased flexibility of the microfibril (Reinhardt et al., 1997; Downing et al., 1996; Cardy and Handford, 1998).

Thurmond and Trotter (1996) reported a near-linear stress–strain relationship of a fibrillin-rich network residue

obtained by extraction of collagen and proteoglycans from sea cucumber (*Cucumaria frondosa*) dermis. However, it is not known how much of the stress–strain properties of this preparation come from the deformability and reorientation of the network as opposed to the deformation of the microfibrils themselves. Similarly, Lillie et al. (1998) studied the properties of a microfibrillar network isolated from pig aorta by digestion with dithiothreitol and guanidine hydrochloride or hot NaOH. Again, the properties of the network contributed to the measured properties. McConnell et al. (1996) estimated the modulus of elasticity of microfibrils in lobster aorta by linear interpolation between the microfibrillar strain in arteries fixed at high *versus* low pressures. However, there are insufficient data points at intermediate values of stress and strain in their study to justify the conclusion of a linear relationship between stress and strain.

We have previously used X-ray diffraction and electron microscopy to study the organisation and deformability of microfibrils in bovine zonular filaments (Wess et al., 1997, 1998a,b). X-ray diffraction data reveal multiple meridional diffraction peaks from structures principally aligned along the axial direction of the zonular filaments (i.e. radiating out from the lens in the eye) which index with a periodicity of 56 nm. Addition and removal of Ca^{2+} produces a reversible change in the intensities of these meridional diffraction peaks. When Ca^{2+} is present, the dominant diffracting subspecies are microfibrils aligned with a 0.33*D* axial stagger. However, only a proportion of the microfibrillar mass contributes to the staggered junctions. Removal of Ca^{2+} causes a more uniform *D* period spacing along individual microfibrils and decreases the dominance in the X-ray pattern of the staggered junction-zone-like arrays. More recent X-ray results show that the effect of strain on the tissue is to enhance the lateral packing of the 0.33*D* staggered zones, without changing the axial periodicities of the bead–interbead region within them to any great extent (Wess et al., 1998a). However, changes in the 56 nm periodicity along the microfibrils in response to applied strain are more apparent in the absence of Ca^{2+}.

The aims of the studies reported in this paper are to measure the load-extension behaviour of zonular filaments from the bovine eye and to explain this behaviour in terms of the molecular and supramolecular organisation of fibrillin-rich microfibrils within the zonular filaments as determined by X-ray diffraction. The predominantly axial alignment of the microfibrils within the zonular filaments makes this tissue useful because the mechanical properties of the tissue are not likely to be as dominated by network orientation phenomena as are the fibrillin-rich tissues previously studied in sea cucumber dermis (Thurmond and Trotter, 1996) and lobster aorta (McConnell et al., 1997).

Materials and methods

Sample preparation

Preparation of zonular filament specimens followed the method of Wess et al. (1997). Briefly, eyes from 18- to 24-month-old Friesian-cross cattle were obtained within 2 h after slaughter and frozen at −20 °C until use. Thawed eyes were opened by circumferental incision to the posterior chamber, and the lens plus ciliary body assembly was removed together with the vitreous humour. Following enucleation of the lens, rectangular frames of thick aluminium foil with interior aperture dimensions of approximately 5 mm×2–3 mm were glued at either end using cyanoacrylate adhesive onto the annulus of zonular filaments with the long axis of the aperture aligned parallel with the radially arranged zonular filaments. The internal dimensions of the frame define the specimen size for mechanical testing. Specimens glued to the frames were then released by dissection around the frame and careful trimming of attached vitreous humour. Remaining vitreous humour was removed by incubating each framed specimen in 2 ml of phosphate-buffered saline (PBS: 150 mmol l^{-1} NaCl, 10 mmol l^{-1} Na_2HPO_4, 2.66 mmol l^{-1} NaH_2PO_4, pH 7.2) or Tris-buffered saline (TBS: 100 mmol l^{-1} NaCl, 5 mmol l^{-1} $CaCl_2$, 50 mmol l^{-1} Tris, pH 7.2) containing 10 mg of bovine testicular hyaluronidase (Sigma) for 8 h at room temperature (22–24 °C), followed by several washes in PBS or TBS. The framed specimens were then frozen flat in a thin film of PBS or TBS and held at −20 °C until use. We have previously found (Wess et al., 1998b) that the Ca^{2+}-binding effects of phosphate in PBS are reversible when specimens are suspended in TBS containing 50 mmol l^{-1} Ca^{2+}.

X-ray diffraction

X-ray diffraction experiments were carried out on beamline 2.1 at the Central Laboratories Research Council (CLRC) Daresbury Laboratory, UK, and on the ID02A small-angle scattering beamline at the European Synchrotron radiation Facility (ESRF) in Grenoble, France. At Daresbury, diffraction data were collected over a 5 min exposure period on a two-dimensional gas-filled detector developed at the CLRC laboratory, with a specimen-to-detector distance of 6.25 m and an X-ray beam spot size at the specimen of 1 mm×2 mm, as defined by slits. The radiation used was of wavelength 0.1488 nm. Specimens on their original frames were sandwiched between thin layers of X-ray-transparent mica, together with a thin film of PBS or TBS, and the mica sheets were sealed at the edges using silicone grease. Specimens were stretched in some cases by cutting the long sides of the aluminium frames, extending the specimen axially and regluing the specimen onto an intact aluminium frame with a longer internal aperture. At ESRF, the sample was mounted in a manner identical to that at the Daresbury Laboratory. Data were collected over 30 s for each exposure using a highly parallel X-ray beam with minimal divergence; the beam at the sample was approximately 100 nm in diameter. The sample-to-detector distance was 5 m for the data shown and the radiation wavelength 1.0 nm. In both cases (CLRC and ESRF data), X-ray data analysis was carried out as described by Wess et al. (1998a,b).

Thickness measurement

For mechanical tests, a measurement of the thickness of the zonular preparations was necessary. This was achieved by

calibrating the focal position control of a Leica DMIL microscope in conjunction with a Leica L32/0.40 objective by focusing on the top and bottom surfaces of single and stacked glass coverslips whose thickness had been measured using a micrometer. The surfaces of zonular filament samples were lightly decorated with fine particles of an inert powder (molybdenum disulphide: Sigma), and thickness was measured as the distance between the focal positions at the top and bottom surfaces. This was repeated seven times. Typically samples were 45–55 μm thick.

Mechanical testing

Cyclic extensions

Tensile tests at a constant deformation rate applied axially to the zonular filaments were carried out in a microscope-mounted microtensiometer of the same general construction and operating characteristics as those described by Mutungi et al. (1995). Load and extension data were acquired *via* a 16-bit A/D converter (National Instruments DAQ 700) and LabView software (National Instruments) on a PC. The smallest resolvable load difference on the apparatus is typically 0.1 mg with the configuration used here. Before testing, the length and width of each specimen were measured using vernier calipers, and the thickness was measured as described above. The frame-mounted specimens were then inserted between the screw-up grips of the tensiometer under a bathing solution of PBS. After gripping was completed, the long sides of the aluminium frame were cut. A mechanical conditioning sequence was applied by extending the sample at 20 mm min^{-1} until a load of 1 g was reached and then returning the sample to zero load at the same deformation rate. The sample was then cycled between loads of 0 and 1 g a further five times to produce a repeatable load–deformation curve in both the loading and unloading phases of the cycle. After this conditioning procedure, the sample was cycled one further time, and this cycle was taken to represent the stable baseline mechanical behaviour of the sample in PBS. Tests were carried out at room temperature (typically 22–24 °C).

Effect of bathing solution

Fifteen samples were mechanically conditioned as described above and then taken through the bathing solutions listed in Table 1 in turn. Two cycles of extension between loads of 0 and 1 g were recorded in each solution. At each change of bathing medium, the sample chamber (capacity approximately 20 ml) was emptied and refilled three times with a complete change of new solution, and the specimen was left to equilibrate for at least 2 min in the final change of solution before testing.

Guanidine treatment

To compare the mechanical behaviour of our preparation with that of Thurmond and Trotter (1996), who used guanidine and dithiothreitol (DTT) in specimen preparation, the following procedure was used on two specimens. Samples were bathed in 6 mol l^{-1} guanidine hydrochloride (GnHCl) in PBS for 16 h after mechanical preconditioning and then washed thoroughly in PBS. Each sample was mechanically cycled twice in PBS, and then cycled twice in TBS containing 15 mmol l^{-1} Ca^{2+} and then in TBS+EGTA (see Table 1). One of the samples was subsequently bathed in PBS containing 0.1 mol l^{-1} DTT, washed thoroughly in PBS and again mechanically cycled twice in PBS. This sample was again cycled twice in high $[Ca^{2+}]$-containing (15 mmol l^{-1}) TBS and in TBS+EGTA. The aim of this procedure was to investigate any irreversible effects that GnHCl or DTT may have had on the preparations.

Table 1. *Chemical composition of buffers (all at pH 7.2)*

	$[Na_2HPO_4]$ (mmol l^{-1})	Tris (mmol l^{-1})	NaCl (mmol l^{-1})	$[CaCl_2]$ (mmol l^{-1})	[EGTA] (mmol l^{-1})
PBS	10 2.66		150		
TBS	50	50	100	5	
High-$[Ca^{2+}]$ TBS	50	50	80	15	
TBS+EGTA	50	50	100		10

PBS, phosphate-buffered saline; TBS, Tris-buffered saline.

Stress-relaxation tests

Two specimens were pre-conditioned in PBS as described above and then extended at 20 mm min^{-1} to a load of 1 g. When this load was reached, the extension was held at this level and the subsequent decay in load over time was recorded.

Extension to failure

Ten samples were extended at 20 mm min^{-1} without pre-conditioning until complete rupture of the sample occurred.

Results

X-ray diffraction

X-ray diffraction data obtained at Daresbury using a relatively large spot size showed different degrees of lateral association of staggered junction zones in a number of specimens, consistent with the hypothesis that there was considerable variation in the pre-strain of different samples. This is demonstrated by comparing the diffraction patterns of two samples at their initial length (Fig. 1A,B). The more pronounced equatorial diffraction maxima in Fig. 1B is evidence of the greater lateral register of the microfibril assemblies in this specimen. Both patterns, however, have meridional diffraction maxima indexing on 56 nm, with strong reflections at spacings corresponding to 56/3 nm. Extension of these two specimens by approximately 50 % of rest length results in the X-ray patterns shown in Fig. 1C,D, respectively. The angular dispersion of the meridional reflections decreases between the initial and stretched state for the sample with the least apparent pre-strain (Fig. 1A,C), showing some improvement of axial alignment of the structures. This

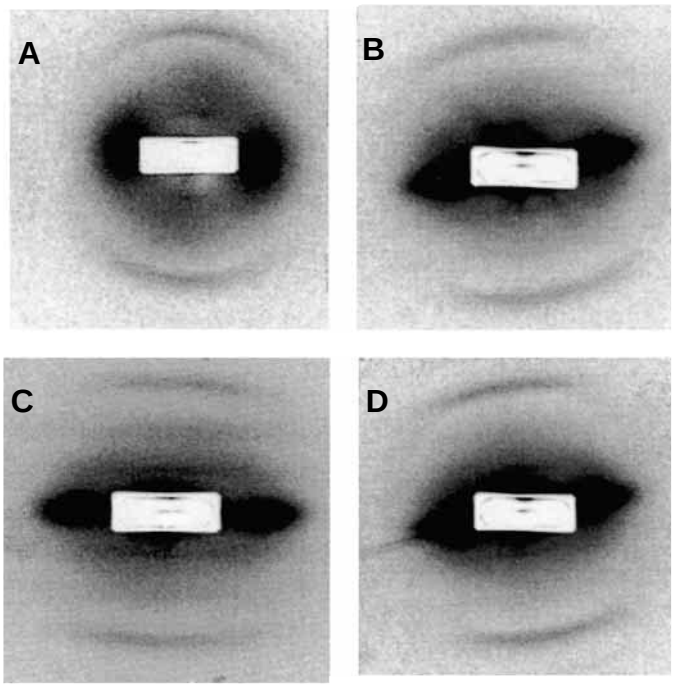

Fig. 1. Small-angle X-ray diffraction patterns from two specimens (A,B) showing different degrees of structural ordering at initial length. Extension by approximately 50 % of the specimen in A results in increased ordering (C), but similar extension of the specimen in B results in little change (D).

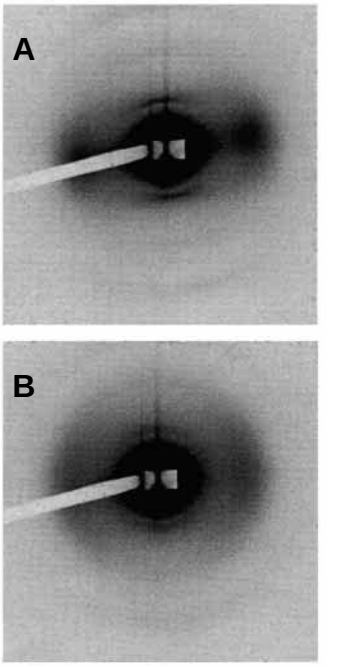

Fig. 2. Microfocus (100 µm spot size) small-angle X-ray diffraction patterns from two different areas (A,B) on the same zonular filament preparation at rest length. (A) Relatively ordered/strained area; (B) less well-ordered area.

specimen also shows an increased intensity of equatorial reflection, indicating increased lateral ordering of molecular assemblies, but only insubstantial changes in the position of the meridional diffraction maxima. The more pre-strained sample shows little change in the diffraction patterns upon extension (Fig. 1B,D). Again, there is no significant change in the position of the meridional reflections.

The small spot size (100 µm) of the ESRF microfocus camera allows local heterogeneities in the specimen to be explored. Fig. 2A,B represent two diffraction patterns taken from a specimen bathed in TBS at rest length. There are quite clear differences in the equatorial diffraction patterns (corresponding to lateral ordering) which are consistent with the idea that there are variations in pre-strain from place to place within the specimen.

Mechanical testing

The first six cycles (i.e. the conditioning cycles) for a typical sample tested in PBS are reproduced in Fig. 3. The J-shaped stress–strain curve shows progressive strain softening at low loads (toe region) but maintains a high stiffness at large stresses. The hysteresis in the first cycle is substantially reduced in subsequent cycles. In all samples, the loop for the seventh cycle overlies that for the sixth. In all these respects, the tissue shows a conditioning behaviour common to many non-linear biological materials (Fung, 1981).

Individual stress–strain curves in PBS for each of the samples tested were similar in shape, but the transition between the compliant toe region and the upper part of the curve (where a higher modulus in displayed) occurred at different levels of strain. This implies some variation in pre-strain in the samples initially. An average stress–strain curve was constructed as follows by compensating for this variation in pre-strain. An estimate of the pre-tension in zonules in the resting eye (see Appendix) was made, and from this a load of 0.1 g chosen to represent the resting load in zonular specimens of the typical dimensions used here. This load was taken as the reference load for which the strain in the sample should be equated to zero. All measured strains in the samples were re-scaled according to this reference, which brought the curves into register. An average of the stresses at various (normalised) strain values was then calculated. The resulting curve is shown in Fig. 4 (curve *a*, in which bars represent standard errors of the stress values at each strain). Curves *b* and *c* illustrate the results for the least- and most-compliant samples in this data set respectively.

Effect of bathing medium

The effects of the bathing media detailed in Table 1 (principally differing in Ca^{2+} concentration) on the properties of a representative zonular specimen are shown in Fig. 5. Curves *a–e* are drawn with successive offsets of 10 % strain for clarity, but in reality they all overlie each other. The mechanical properties of the specimen tested in PBS (curve *b*), TBS (curve *c*), high-[Ca^{2+}] TBS (curve *d*) and TBS+EGTA (curve *e*) appear unchanged by the composition of the bathing medium. The average stress–strain curve in PBS is drawn as

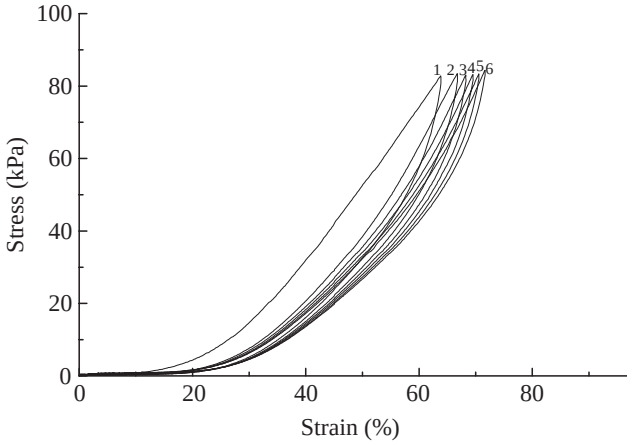

Fig. 3. Stress–strain diagram showing pre-conditioning cycles 1–6 for a typical specimen.

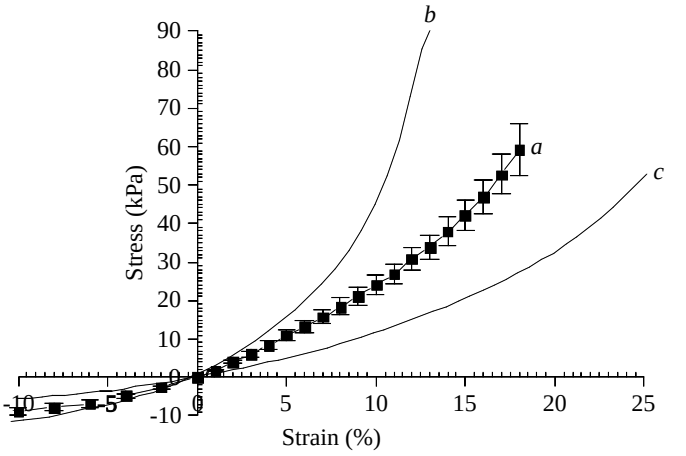

Fig. 4. Curve *a* is the mean stress–strain curve calculated from the load-elongation data for 11 samples. Values are means ± S.E.M. Curve *b* is the stress–strain curve for the least compliant sample. Curve *c* is the stress–strain curve for the most compliant sample.

(negatively offset) curve *a* to illustrate that the sample chosen is a typical one. The same insensitivity of the deformation behaviour to the bathing solution was found for 15 other samples tested (in strain cycling experiments) without GnHCl treatment in this study.

The effect of 6 mol l^{-1} GnHCl on stress–strain behaviour is demonstrated in Fig. 6. Curve *a* shows two cycles, prior to treatment, in PBS. Curve *b* shows two cycles obtained in Ca^{2+}-deficient buffer (TBS+EGTA) subsequent to GnHCl treatment. After treatment in GnHCl, bathing in a high [Ca^{2+}]-containing buffer resulted in stress–strain behaviour overlying curve *a*, whilst bathing in the EGTA-containing medium resulted in stress–strain behaviour overlying curve *b*. Moreover, this effect was reversible. However, when the same sample was treated with 0.1 mol l^{-1} DTT following GnHCl treatment and subsequently bathed in high-[Ca^{2+}] TBS, the stress–strain behaviour did not revert to that described by curve *a*, i.e. the effect was not reversible.

The overall extensibility of the aligned microfibril assemblies in the zonules was found to be less than reported previously for distributed networks of microfibrils (Thurmond and Trotter, 1996), as shown from the stress–strain curve for a sample strained to failure (Fig. 7). The curve is initially J-shaped with a gradual transition from a low-modulus region into a linear high-modulus region at approximately 30 % strain. However, failure in this sample starts to occur at only 60 % strain and continues until complete rupture of the specimen occurs at 140 % strain. Microscopic examination of the samples during failure showed that the rupture of zonular filaments coincided with troughs on the saw-tooth part of the curve. The shape of this curve is typical of those tested to failure in this investigation. The sample depicted in Fig. 7 had a relatively low failure strain, but others showed values up to 300 %. This variability is again consistent with the concept that different specimens had varying levels of pre-strain in the initial state.

The relaxation modulus (stress/strain) as a function of time for a typical sample is illustrated in Fig. 8. A rapid decay in modulus is observed over the first 20 s, followed by a more gradual decay thereafter. Restitution of the sample to its original length results in stress recovery. These findings indicate that at least some of the deformation behaviour of the zonules is not purely elastic, but viscoelastic.

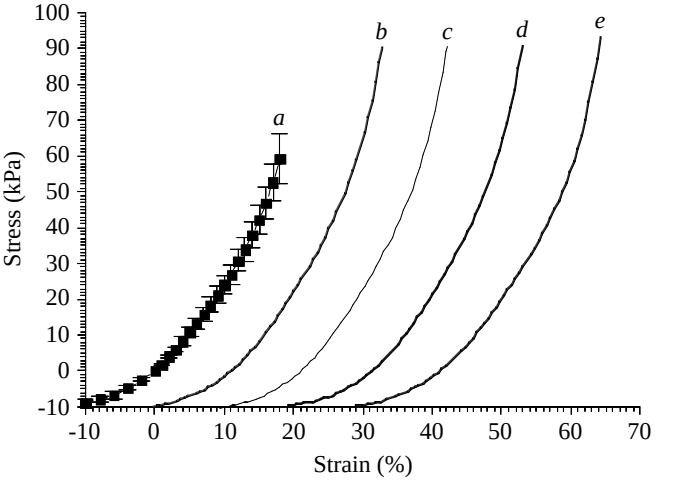

Fig. 5. Comparison of stress–strain behaviour of a typical sample in different buffers. Curve *a* is the average stress–strain curve. Values are means ± S.E.M., *N*=11. Curve *b* is for a sample tested in phosphate-buffered saline. Curve *c* is for a sample tested in Tris-buffered saline (TBS). Curve *d* is for a sample tested in high-[Ca^{2+}] TBS. Curve *e* is for a sample tested in TBS+EGTA (see Table 1). Curves *c*, *d* and *e* have been sequentially offset (displaced) by +10 % strain with respect to the previous curve on this figure. Curve *a* (the average stress–strain curve from Fig. 4) is drawn translated by −10 % strain relative to curve *b*. These translations are so that each curve can be clearly seen; in reality, the five curves are all superimposed.

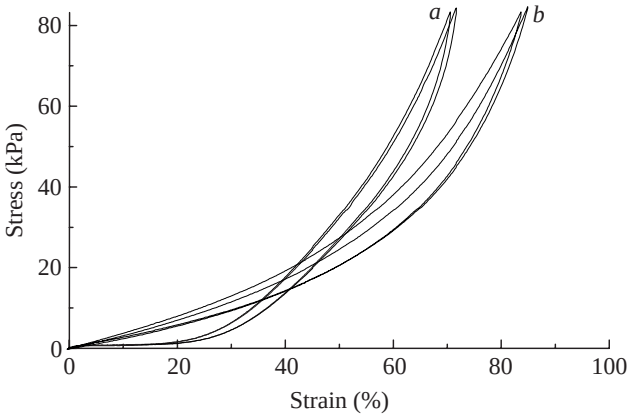

Fig. 6. The effect of treatment with guanidine hydrochloride on the stress–strain behaviour of a sample of zonule (curve *a*) in PBS and (curve *b*) in TBS+EGTA. Two stress–strain cycles are shown for each treatment. Subsequent bathing in high [Ca^{2+}]TBS reverts the behaviour to that in curve (a). The effects of addition/removal of Ca^{2+} are reversible.

Discussion

Previous papers concerning the mechanical properties of networks of fibrillin-rich microfibrils (Thurmond and Trotter, 1996; McConnell et al., 1996, 1997) give the impression of highly extensible and near-linear stress–strain behaviour in some ionic environments. The mechanical behaviour of the fibrillin-rich zonular filaments reported here differs somewhat in that the stress–strain curve is more noticeably J-shaped (even though the zonular filaments are aligned with the stretching direction) and ultimate extensibility appears a little lower. The mechanical protocols and results in this current study have been laid out in detail in an attempt to aid discussion of why some of these differences occur.

Thurmond and Trotter (1996) extracted their fibrillin-rich network from sea cucumber dermis after extensive extraction of other components in the tissue with crude collagenase and 6 mol l^{-1} GnHCl to extract collagen fibrils. It is possible that non-specific protelytic activity in some crude collagenases may result in microfibrils being more extensible than normal (C. M. Kielty, unpublished results). They also examined the effect of DTT on the properties of this material. We included a guanidine treatment in our protocols to investigate the effect of this denaturation. From Fig. 6, it is clear that GnHCl treatment makes the zonules more compliant to a 1 g load but introduces a more linear toe region to the stress–strain curve. However, the stress–strain curve is still J-shaped. Disruption of disulphide bonds by DTT subsequent to GnHCl treatment further increases the compliance of our preparation, but this effect is not reversible when samples are resuspended in fresh PBS, as is the case with guanidine. It appears, therefore, that at least some of the compliance seen by Thurmond and Trotter (1996) may be due to their extraction procedure. Unpublished X-ray diffraction data (T. J. Wess and P. P. Purslow) also indicate that the addition of 4 mol l^{-1} GnHCl causes the Bragg peaks to be lost from the fibre diffraction pattern, but reincubation in PBS allows the diffraction to recover to a level comparable with the diffraction signal above the noise level prior to GnHCl treatment.

There are a number of mechanisms that can explain a J-shaped stress–strain curve for uniaxially strained tissues. One common mechanism is strain-induced reorientation of load-bearing elements or reinforcing fibrils. Reorientation occurs as a result of the difference in strains along the three orthogonal principal axes; in a uniform biaxial stress field that exists in the sclera of the eye due to intraocular pressure, for example, no reorientation of collagen fibres in the plane of the scleral wall is expected with increasing pressure because the resultant circumferential strains are equal in all directions. Fibre reorientation is seen in a number of matrices, and the increasing stiffness with increasing strain of skin (Veronda and Westmann, 1970), various mammalian blood vessel walls (Roveri et al., 1980; Bigi et al., 1981), intervertebral disc (Klein and Hukins, 1982), perimysium (Purslow, 1989) and endomysium (Purslow and Trotter, 1994) has been quantitatively explained by reorientation of collagen fibres in these matrices. Lillie at al. (1998) conclude that reorientation and straightening of microfibrils is probably a major mechanism behind the non-linear stress–strain curves they measured on alkali-treated or DTT-digested aortae.

McConnell et al. (1997) equate the reorientation of fibrillin-rich microfibrils in lobster aortae fixed at different pressures to the J-shaped stress–strain curve obtained for this tissue. Reorientation occurs in pressurised blood vessels because of the difference in strains along the circumferential *versus* the longitudinal directions. However, in the zonular filaments studied here, the fibrillin-rich microfibrils are macroscopically aligned with the stretching direction to start with, so that this mechanism does not seem to be a major possible contributor to the mechanical behaviour observed. It is also possible the J-shaped curve is due to the presence of a non-fibrillin component, e.g. a collagen network. However, treatment of the zonular preparation used in this study with collagenase affects neither the X-ray nor the mechanical behaviour (results not shown). There is also no evidence for collagen fibrillar diffraction in the X-ray diffraction data.

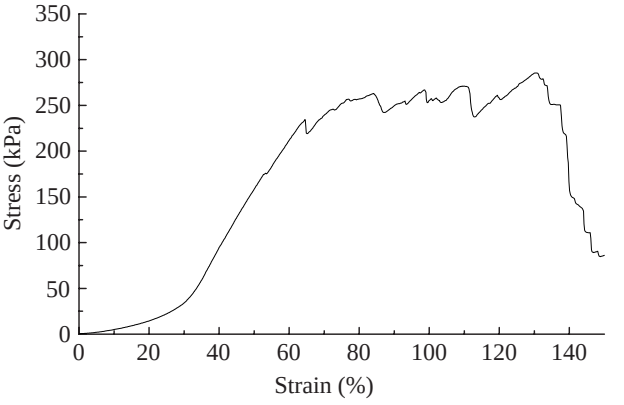

Fig. 7. Stress–strain curve for a zonular filament sample strained to failure.

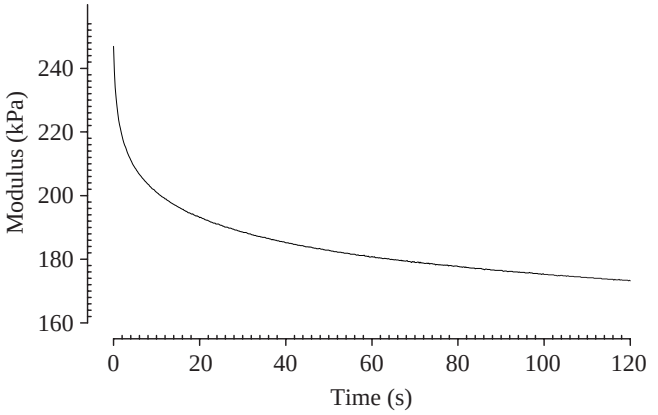

Fig. 8. Stress-relaxation behaviour of a zonular filament sample. Relaxation modulus (stress/strain) *versus* time for a specimen held at fixed extension after extension at 20 mm min^{-1} to a load of 1 g.

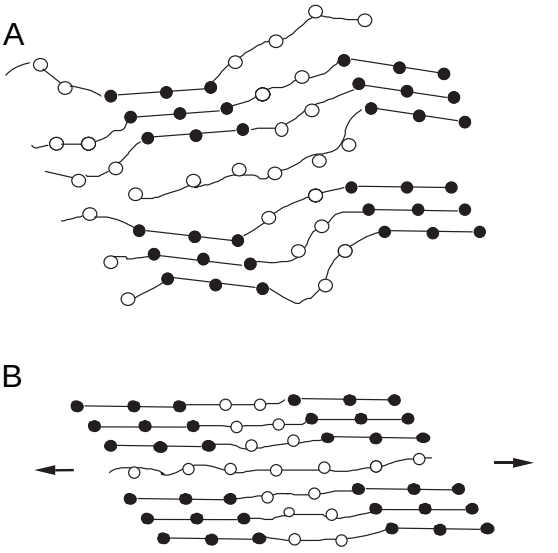

Fig. 9. Schematic diagram of microfibril arrays in zonular filaments unstretched (A) and stretched in the direction of the arrows (B). Microfibrils are represented as 'beads on string' structures. Black beads denote regions of each microfibril participating in one-third stagger overlap with neighbouring microfibrils. The action of stretch is to increase the order of the regions not involved in such staggered arrays.

In tissues containing macroscopically aligned fibres, a J-shaped stress–strain curve can be explained in terms of straightening of the wavy parts of the fibres on stretching. This mechanism has long been put forward to explain the J-shaped stress–strain curve of tendons resulting from straightening of uniformly wavy (but aligned) collagen fibres in response to applied strain (Diamant et al., 1972; Kastelic et al., 1980). This explanation inherently contains the idea that high loads are only borne in straight fibres, which have a higher tensile modulus than wavy ones. The microfibrils seen in unstressed dorsal abdominal artery of the lobster are wavy, but straighten out in a pressurised vessel (Fig. 1 in McConnell et al., 1996). Decreased waviness upon straining also increases the lateral alignment of adjacent fibres (Fig. 1 in McConnell et al., 1996). This is analogous to the increased regularity of lateral packing between microfibrils in zonular filaments under strain, resulting in more intense and defined equatorial diffraction maxima in X-ray studies (Fig. 2 in the present study; Fig. 1 in Wess et al., 1998a).

A third mechanism to explain J-shaped stress–strain behaviour is the presence of a distribution of degrees of waviness in aligned fibres. Kastelic et al. (1980) and Decraemer et al. (1980) use this idea to model the J-shaped stress–strain curves of a number of tissues. Fibres with a higher degree of waviness will require greater axial strains to straighten them than their less wavy neighbours. Thus, increasing strain gradually recruits a higher proportion of straight (and maximally stiff) fibres. There are a number of attractive features of this model in connection with the present study on zonular filaments. As shown by Fig. 1, different degrees of pre-strain can exist within one zonular filament preparation. The effect of axial extension to 50 % of zonular filaments is to increase the intensity above background of Bragg reflections corresponding to a 56/3 nm spacing, indicating an increased order or uniformity in this axial spacing (Wess et al., 1998b), which may correspond to an increased ordering of the axial spacing as microfibrillar assemblies are straightened out.

It is clear from both the X-ray results and the mechanical results reported here that there is variability in the pre-strain in zonular filament preparations isolated from bovine eyes. In part, the procedure of gluing regions of the zonules onto aluminium frames before excision is an attempt to preserve some initial unstressed state of the material. However, the *in vivo* resting state of the eye, with a carefully controlled intraocular pressure, has long since been disturbed by the time that the zonular apparatus is accessible for dissection. This problem (loss of resting *in vivo* pre-tension) is common in work on tissues such as skin and the major arteries. *In vivo* it is possible that the zonules are pre-tensioned above the 'toe' region of the J-shaped stress–strain curve. It has been pointed out to us that small amounts of non-specific proteolytic activity may occur in our hyaluronidase incubations and this may add somewhat to the variability in properties between specimens. However, it is clear that the non-linear response of the tissue in general is due to some increased ordering of microfibrillar assemblies in response to axial strain.

Wess et al. (1998b) show that the meridional diffraction patterns from fibrillin-rich microfibrils in the zonular filaments in the presence of Ca^{2+} can be modelled by arranging 90 % of the diffracting mass into laterally aligned aggregates with a 0.33*D* axial stagger between adjacent microfibrils, with the remaining 10 % of the microfibrillar mass non-aligned, i.e. more disordered. It must be stressed that this 90:10 ratio of aligned and unaligned molecular structures corresponds to their contribution to the diffraction data and not necessarily their overall mass-fraction. It is highly likely that there is a significant portion of the zonular structure where a lack of

molecular coherence (even within a single beaded filament) would mean that no contribution was made to Bragg diffraction from that part of the sample, whereas such a region could be contributing to the elasticity of the sample. In the presence of EGTA, Wess et al. (1998b) calculate that 65 % of the diffracting mass is in aligned aggregates, with 35 % non-aligned. Making the assumption that the laterally aligned aggregates with a 0.33*D* axial stagger are less deformable than the more disordered regions, it is possible to explain the changes in diffraction patterns and mechanical properties on extension of the tissue in terms of the strain-induced ordering of the non-aligned, less-ordered parts of the microfibrils. This concept is illustrated schematically in Fig. 9. The proportion of non-aligned regions in this diagram is exaggerated to show the proposed mechanism clearly.

The mechanical properties of the zonule are best described as viscoelastic (time-dependent) rather than purely elastic, as demonstrated by the strong stress-relaxation behaviour shown in Fig. 8. In sea cucumber dermis, the complementary viscoelastic phenomena of creep compliance and delayed strain recovery can be seen (Thurmond and Trotter, 1996**)**. The molecular basis of viscoelastic deformations in fibre-reinforced extracellular matrices is not well understood, but does not seem to be related to realignment or reorientation of the fibrils, at least in the case of two collagenous tissues (Purslow et al., 1998). It should be noted that the rates of extension used here (20 mm min^{-1} for a typical gauge length of 5 mm) are slow compared with *in vivo* loading rates, but faster than those used by Thurmond and Trotter (1996), who measured near-equilibrium force values after low stretches. It is therefore possible that our results contain a greater contribution from viscous mechanisms that have relaxation times slower than our loading rate.

Kielty and Shuttleworth (1997) report that incubation of microfibrils in 4 mol l^{-1} GnHCl results in a disrupted interbead morphology. They also state that these denatured microfibrils have a more curvilinear configuration (flexible structure) on the surface of mica than native microfibrils observed by rotary shadowing. GnHCl-treated microfibril material equilibrated in deionised water by Thurmond and Trotter (1996) had a disrupted interbead morphology when viewed by rotary shadowing, whereas specimens equilibrated in artificial sea water containing Ca^{2+} had an ordered interbead morphology. This observation is consistent with the more compliant response to the application of a 1 g load seen in GnHCl-treated zonules reported in Fig. 6.

Samples treated with DTT showed a disrupted microfibril morphology observed by rotary shadowing even after being equilibrated in Ca^{2+}-containing artificial sea water (Thurmond and Trotter, 1996). Thurmond and Trotter equate this permanent disruption to the reduction of disulphide bonds within the epidermal growth factor-like domains of fibrillin, destroying the Ca^{2+}-binding properties (eight cysteine motifs are probably involved in intermolecular disulphide crosslinking). This is possibly why the effects of Ca^{2+} removal could not be reversed in this investigation after DTT treatment.

Ca^{2+} has previously been shown to modulate the axial repeat (*D* period) and distribution of mass between bead and interbead regions of the *D* period, as examined by scanning transmission electron microscopy, of hydrated intact microfibrils within the arrays found in zonular filaments (Wess et al., 1998b). Previous studies on dehydrated microfibrils using rotary shadowing (Kielty and Shuttleworth, 1993) have shown that Ca^{2+} removal disrupts the packing of the molecules within the interbead domains of the microfibril without affecting interbead periodicity and that this disruption is reversed by reintroducing Ca^{2+}. Whilst this may lead to an expectation of different extensibilities of fibrillin-rich tissue when Ca^{2+} is removed, no evidence of any change in the mechanical properties of zonular filaments in the presence or absence of Ca^{2+} was observed here. This is in contrast to the observations of Thurmond and Trotter (1996), who noted an increased compliance of their fibrillar network in water compared with artificial sea water containing 10 mmol l^{-1} $CaCl_2$. However, this may be an effect of hypotonicity rather than a specific ion effect. Wess et al. (1998b) demonstrate that, in zonular filaments containing aggregated and staggered aligned arrays of microfibrils, there is a change in the supramolecular organisation, as shown by changing intensities of the orders of X-ray diffraction peaks indexing at a periodicity of 56 nm. In the presence of Ca^{2+}, the dominant diffracting structures are the 0.33*D* staggered overlap regions of the microfibrils, whilst the regions between the staggered arrays appear to contain less well-ordered bead–interbead distances. Removal of Ca^{2+} appears to reduce the contribution of the staggered arrays to the diffraction pattern and enhance the regularity of the bead–interbead spacings along the microfibrils. The axial spacing demonstrated within the staggered regions does not change significantly on extension of the zonules, which suggests that these aggregates are relatively stiff. However, some indications of large extensions in the *D* periodicity can be found in highly extended specimens, where the 0.33*D* stagger arrangement is lost (Wess et al., 1998a). The X-ray studies reported here are consistent with these previous reports.

There are several explanations for the non-sensitivity of the stress–strain curve of zonular filaments to Ca^{2+}. First, it may be that, although the molecular structure of individual microfibrils changes with Ca^{2+} concentration, the mechanical properties do not. Second, it may be that the supramolecular arrays of microfibrils do not show Ca^{2+}-sensitive properties because their properties are dominated by structures not present in single microfibrils. Third, it may be that the mechanical properties of this tissue are dominated by the properties of some component other than the high concentration of fibrillin-rich microfibrils that make up the bulk of the tissue (in which event, the structural basis of elasticity of the microfibrils would be irrelevant to the functioning of the tissue that contains them). Together with the mechanical investigations, the X-ray data presented here and in previous work (Wess et al., 1998a,b) suggest the second option, i.e. that the properties of the tissue as a whole may be dominated by the aligned staggered assemblies of microfibrils,

which are brought into increasing register by applied strain. Aggregated arrays of aligned microfibrils are easily seen by transmission electron microscopy in zonular filaments (Wess et al., 1998b), but less easily seen in lobster aorta (McConnell et al., 1996) or sea cucumber dermis (Thurmond and Trotter, 1996). It could be that the non-aggregated microfibrils of these tissues demonstrate *D* period extension more easily and are more compliant. The pattern of lateral striations seen by Davison et al. (1995) in aligned groups of fibrillin-rich fibrils in whelk aorta may indicate a regular, staggered packing of microfibrils in this tissue also. The modulus of elasticity measured for whelk aorta is 3–6 times higher than that of lobster aorta, depending on measurement temperature (Davison et al., 1995). Although this difference is probably due to a radically different morphology in the aortae of whelk *versus* lobster, it is also possible that aligned assemblies of microfibrils may also be less extensible. To test whether the mechanical properties of aligned arrays of microfibrils are indeed different from those of smaller aggregates or individual fibrils, micromechanical tests at the molecular/near molecular level are required.

Appendix

Calculation of zonular pre-tension from intraocular pressure in vivo

The intraocular pressure (P) imposes a circumferential stress (σ) on the ocular shell. Simple analysis of the eyeball as a thin-walled pressure vessel of elastic, homogeneous and isotropic material yields the following relationship (Purslow and Karwatowski, 1996):

$$\sigma = PR/t_c . \quad (1)$$

The radius, R, of the bovine eye ball is typically 15 mm, and the corneal thickness, t_c, is approximately 1 mm. The intraocular pressure, P, is between 1 and 4 kPa. An estimate of the preload f_{pl} in kilograms that needs to be applied to a sample of zonular membrane of thickness t and width w can be obtained from equation 2 using the value of stress from equation 1 and the acceleration due to gravity, g.

The value 0.1 g is a low but reasonable estimate for the pre-tension in a typical zonular filament preparation:

$$f_{pl} = \frac{\sigma wt}{g} = \frac{PRwt}{t_c g} . \quad (2)$$

We wish to thank A. Gleeson and G. Grossmann for their assistance in setting up and operating the X-ray diffraction facilities at CLRC and also T. Narayanan, J. Orgel and A. Hammersley for help with data collection at on beamline ID02A ESRF. The support of the Wellcome Trust (D.M.W.) is gratefully acknowledged.

References

Bigi, A., Ripamonti, A., Roveri, N., Jeronimidis, G. and Purslow, P. P. (1981). Collagen orientation by X-ray pole figures and mechanical properties of media carotid wall. *J. Mater. Sci.* **16**, 2557–2562.

Cardy, C. M. and Handford, P. A. (1998). Metal ion dependency of microfibrils supports a rod-like conformation for fibrillin-1 calcium-binding epidermal growth factor-like domains. *J. Mol. Biol.* **276**, 855–860.

Davison, I. G., Wright, G. M. and Demont, M. E. (1995). The structure and physical properties of invertebrate and primitive vertebrate arteries. *J. Exp. Biol.* **198**, 2185–2196.

Decraemer, W. F., Maes, M. A. and Vanhuyse, V. J. (1980). An elastic stress–strain relation for soft biological tissues based on a structural model. *J. Biomech.* **13**, 463–468.

Diamant, J., Keller, A., Baer, E., Litt, M. and Arridge, R. G. C. (1972). Collagen: ultrastructure and its relation to mechanical properties as a function of aging. *Proc. R. Soc. Lond. B* **180**, 293–315.

Downing, A. K., Knott, V., Werner, J. M., Cardy, C. M., Campbell, I. D. and Handford, P. A. (1996). Solution structure of a pair of calcium-binding epidermal growth factor-like domains: implications for the Marfan syndrome and other genetic disorders. *Cell* **85**, 597–605.

Fung, Y. C. (1981). *Biomechanics: The Mechanical Properties of Living Tissues*. pp. 219–220. Berlin: Springer-Verlag.

Gibson, M. A., Hatzinikolas, G., Kumaratilake, J. S., Sandberg, L. B., Nicholl, J. K., Sutherland, G. R. and Cleary, E. G. (1996). Further characterization of proteins associated with elastic fiber microfibrils including the molecular cloning of MAGP-2 (MP25). *J. Biol. Chem.* **271**, 1096–1103.

Kastelic, J., Palley, I. and Baer, E. (1980). A structural mechanical model for tendon crimping. *J. Biomech.* **13**, 887–893.

Keene, D. R., Maddox, B. K., Kuo, H. J., Sakai, L. Y. and Glanville, R. W. (1991). Extraction of extendable beaded structures and their identification as fibrillin-containing extracellular-matrix microfibrils. *J. Histochem. Cytochem.* **39**, 441–449.

Kielty, C. M. and Shuttleworth, C. A. (1993). The role of calcium in the organization of fibrillin microfibrils. *FEBS Lett.* **336**, 323–326.

Kielty, C. M. and Shuttleworth, C. A. (1995). Fibrillin containing microfibrils: structure and function in health and disease. *Int. J. Biochem. Cell Biol.* **27**, 747–760.

Kielty, C. M. and Shuttleworth, C. A. (1997). Microfibrillar elements of the dermal matrix. *Microsc. Res. Tech.* **38**, 413–427.

Kielty, C. M., Whittaker, S. P. and Shuttleworth, C. A. (1996). Fibrillin: Evidence that chondroitin sulphate proteoglycans are components of microfibrils and associate with newly synthesised monomers. *FEBS Lett.* **386**, 169–173.

Klein, J. A. and Hukins, D. W. L. (1982). Collagen fiber orientation in the annulus fibrosus of intervertebral-disk during bending and torsion measured by X-ray-diffraction. *Biochim. Biophys. Acta* **719**, 98–101.

Lillie, M. A., David, G. J. and Gosline, J. M. (1998). Mechanical role of elastin-associated microfibrils in pig aortic elastic tissue. *Connective. Tissue Res.* **37**, 121–141.

Mayne, R., Brewton, R. G. and Ren, Z. X. (1997). Vitreous body and zonular apparatus. In *Biochemistry of the Eye* (ed. J. J. Harding), pp. 135–143. London: Chapman & Hall.

McConnell, C. J., Demont, M. E. and Wright, G. M. (1997). Microfibrils provide non-linear elastic behaviour in the abdominal artery of the lobster *Homarus americanus*. *J. Physiol., Lond.* **499**, 513–526.

McConnell, C. J., Wright, G. M. and Demont, M. E. (1996). The modulus of elasticity of lobster aorta microfibrils. *Experientia* **52**, 918–921.

Mecham, R. P. and Heuser, J. (1991). The elastic fiber. In *Cell Biology of Extracellular Matrix* (ed. E. D. Hay), pp. 79–109. New York: Plenum Press.

Mutungi, G., Purslow, P. and Warkup, C. (1995). Structural and mechanical changes in raw and cooked single porcine muscle-fibers extended to fracture. *Meat Sci.* **40**, 217–234.

Purslow, P. P. (1989). Strain-induced reorientation of an intramuscular connective tissue network: implications for passive muscle elasticity. *J. Biomech.* **22**, 21–31.

Purslow, P. P. and Karwatowski, W. S. S. (1996). Ocular elasticity – Is engineering stiffness a more useful characterization parameter than ocular rigidity? *Ophthalmol.* **103**, 1686–1692.

Purslow, P. P. and Trotter, J. A. (1994). The morphology and mechanical-properties of endomysium in series-fibered muscles: variations with muscle length. *J. Muscle Res. Cell Motil.* **15**, 299–304.

Purslow, P. P., Wess, T. J. and Hukins, D. W. L. (1998). Collagen orientation and molecular spacing during creep and stress-relaxation in soft connective tissues. *J. Exp. Biol.* **201**, 135–142.

Reinhardt, D. P., Keene, D. R., Corson, G. M., Poschl, E., Bachinger, H. P., Gambee, J. E. and Sakai, L. Y. (1996). Fibrillin-1: Organization in microfibrils and structural properties. *J. Mol. Biol.* **258**, 104–116.

Roveri, N., Ripamonti, A., Pulga, C., Jeronimidis, G., Purslow, P. P., Volpin, D. and Gotte, L. (1980). Mechanical behaviour of aortic tissue as a function of collagen orientation. *Makromol. Chem.* **181**, 1999–2007.

Sakai, L. Y., Keene, D. R. and Engvall, E. (1986). Fibrillin, a new 350-kd glycoprotein, is a component of extracellular microfibrils. *J. Cell Biol.* **103**, 2499–2509.

Sakai, L. Y., Keene, D. R., Glanville, R. W. and Bachinger, H. P. (1991). Purification and partial characterization of fibrillin, a cysteine-rich structural component of connective-tissue microfibrils. *J. Biol. Chem.* **266**, 14763–14770.

Sherratt, M. J., Holmes, D. F., Shuttleworth, C. A. and Kielty, C. M. (1997). Scanning transmission electron microscopy mass analysis of fibrillin containing microfibrils from foetal elastic tissues. *Int. J. Biochem. Cell Biol.* **29**, 1063–1070.

Taipale, J., Saharinen, J., Hedman, K. and Keskioja, J. (1996). Latent transforming growth factor-beta 1 and its binding protein are components of extracellular matrix microfibrils. *J. Histochem. Cytochem.* **44**, 875–889.

Thurmond, F. A. and Trotter, J. A. (1996). Morphology and biomechanics of the microfibrillar network of sea cucumber dermis. *J. Exp. Biol.* **199**, 1817–1828.

Veronda, D. R. and Westmann, R. A. (1970). Mechanical characterisation of skin: finite deformations *J. Biomech.* **3**, 111–124.

Waggett, A. D., Kielty, C. M. and Shuttleworth, C. A. (1993). *Proceedings of the 9th Annual Conference of the National Marfan Foundation.* Portland, Oregon, August 1993. (Abstract).

Wess, T. J., Purslow, P. P. and Kielty, C. M. (1997). Fibrillin-rich microfibrils: an X-ray diffraction study of the fundamental axial periodicity. *FEBS Lett.* **413**, 424–428.

Wess, T. J., Purslow, P. P. and Kielty, C. M. (1998a). X-ray diffraction studies of fibrillin-rich microfibrils: Effects of tissue extension on axial and lateral packing. *J. Struct. Biol.* **122**, 123–127.

Wess, T. J., Purslow, P. P., Sherratt, M. J., Ashworth, J., Shuttleworth, C. A. and Kielty, C. M. (1998b). Calcium determines the supramolecular organization of fibrillin-rich microfibrils. *J. Cell Biol.* **141**, 829–837.

Wright, D. W., McDaniels, C. N., Swasdison, S., Accavitti, M. A., Mayne, P. M. and Mayne, R. (1994). Immunization with undenatured bovine zonular fibrils results in monoclonal antibodies to fibrillin. *Matrix Biol.* **14**, 41–49.